Nanoindentation and Cavitation-Induced Fragmentation Study of Primary Al₃Zr Intermetallics Formed in Al Alloys

Abhinav Priyadarshi, Tungky Subroto, Marcello Conte, Koulis Pericelous, Dmitry Eskin, Paul Prentice, and Iakovos Tzanakis

Abstract

Mechanical properties of primary Al₃Zr crystals and their in situ fragmentation behaviour under the influence of a single laser induced cavitation bubble have been investigated using nanoindentation and high-speed imaging techniques, respectively. Linear loading of 10 mN was applied to the intermetallics embedded in the Al matrix using a geometrically well-defined diamond nanoindenter to obtain the mechanical properties at room temperature conditions. Primary Al₃Zr crystals were also extracted by dissolving the aluminium matrix of an Al-3wt% Zr alloy. The extracted primary crystals were also subjected to cavitation action in deionized water to image the fracture sequence in real time. Fragmentation of the studied intermetallics was recorded at 500,000 frames per second. Results showed that the intermetallic crystals fail by brittle fracture mode most likely due to the repeatedly-generated shock waves from the collapsing bubbles. The results were interpreted in terms of fracture mechanics using the nanoindentation results.

A. Priyadarshi (✉) · I. Tzanakis
Faculty of Technology, Design and Environment, Oxford Brookes University, Oxford, OX33 1HX, UK
e-mail: abhinav.priyadarshi-2018@brookes.ac.uk

T. Subroto · D. Eskin
Brunel Centre for Advance Solidification Technology (BCAST), Brunel University London, Uxbridge, UB8 3PH, UK

M. Conte
Anton Paar TriTec SA, Rue de la Gare 4, 2034 Peseux, Switzerland

K. Pericelous
Computational Science and Engineering Group (CSEG), Department of Mathematics, University of Greenwich, London, SE10 9LS, UK

P. Prentice
Cavitation Laboratory, School of Engineering, University of Glasgow, Glasgow, G12 8QQ, UK

D. Eskin
Tomsk State University, Tomsk, 634050, Russia

I. Tzanakis
Department of Materials, University of Oxford, Oxford, OX1 3PH, UK

Introduction

Ultrasonic melt treatment (UST) offers an economical and environment friendly approach to liquid metal processing with benefits of improved cast structure and properties resulting in production of high quality light metal alloys [1]. Specifically, mechanical properties in various aluminium alloys can be significantly altered by the formation and refinement of the primary intermetallic particles. Refined intermetallics can act as reinforcing particles to produce metal matrix composites (MMC's) in Al–Si [2] or Al–Ti alloys [3] systems resulting in considerable improvements in terms of elastic modulus, hardness, thermal stability, low density and high corrosion resistance [4, 5].

Even though the resulting effect of UST on the as-cast metallic alloys is quite reproducible [6, 7], understanding the in situ fragmentation mechanisms of free floating primary crystals is still a work in progress. Research in this field is now considerably enhanced by the possibility of in situ high-speed-optical imaging or X-ray assisted imaging of transparent organic alloys [8–10]. Chow et al. [10] found out that nucleation of grains was considerably enhanced through ultrasonic vibrations and subsequent fragmentation of the dendrites caused by oscillation, and collapse of stable and inertial cavitation bubbles. Wagterveld et al. [11] observed the effect of cavitation bubbles on the fragmentation of suspended calcite crystals in a calcium carbonate solution. It was found out that the fracture of these calcite crystals was initiated by the continuous collapse of formed bubble

clusters. Lately, synchrotron X-ray imaging has been widely applied to the studies of in situ solidification of real liquid metals and alloys under the influence of different external fields [12–15]. Wang et al. [14] investigated the fragmentation of Al_2Cu intermetallic dendrites in an Al-35% Cu alloy by ultrasonic treatment using X-ray radiography. Other studies on alloy melts include the dynamic behaviour of cavitation bubbles in an Al-10wt% Cu alloy [15] as well as interaction between the acoustic bubble/flow and solidifying phases in an Bi-8%Zn alloy [12, 16] Recently, Wang et al. [2] developed an efficient method of observing the real time interaction of ultrasonic induced cavitation bubbles with various primary intermetallic phases such as Si, Al_3Ti, and Al_3V crystals. Although, this work shed some light on the mechanisms of cavitation-induced fragmentation, a discernible gap exists in relating; (1) the relation of the fragmentation of the crystal to its mechanical properties and (2) associated fracture mechanisms caused by the collapsing bubbles. It is believed that a combination of acoustic streaming [14] with liquid jet impingement and shock waves propagation from the collapsed cavitation bubbles are responsible for the fragmentation of crystals in liquid melts; similar to the pitting mechanism on solid surfaces [17]. In this study, we revealed for the first time that fragmentation of intermetallic particles is mainly driven by the propagation of shock waves from the collapsing bubbles.

Specifically, the mechanical properties of primary Al_3Zr crystals extracted from an Al-3%Zr alloy have been evaluated using a depth sensing indentation technique at ambient conditions. Subsequently, fragmentation experiments of extracted Al_3Zr crystals have been conducted in deionized water by laser-induced cavitation with in situ high-speed imaging. Experimental results were explained using stress-fracture mechanics.

Experimental Methodology

Intermetallics Extraction and Sample Preparation

Approximately 350 grams of an Al-3wt% Zr alloy were produced by smelting pure Al (99.97%) and an Al-5wt% Zr master alloy. The formed alloy was re-melted in an electrical furnace and solidified in a cylindrical graphite mould (Ø = 50 mm) with a thermal cycle as illustrated in Fig. 1. $5 \times 5 \times 5$ mm cubes were then cut using a SiC rotating blade out of the ingot.

To extract Al_3Zr intermetallics from the sample, the Al-3wt% Zr, a cube sample was immersed in 15% NaOH water solution for 24 h. Dissolution of Al matrix was carried out through the following chemical reaction:

$$2Al + 2NaOH + 2H_2O \rightarrow 2NaAlO_2 + 3H_2$$
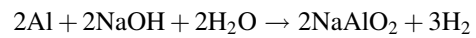
The resulting solution was filtered out and the extracted intermetallics were then collected and thoroughly rinsed using ethanol and left to dry out for the following studies. Figure 2a shows the morphological image of an extracted Al_3Zr crystal. These extracted primary intermetallics exhibit a well-facetted and thin tabular crystals as also observed by Zhen and Davies [18].

Additionally, a part of the cast ingot was cut longitudinally and sectioned along the central axis from the bottom where the primary intermetallics tend to settle during slow cooling because of the high density of Al_3Zr. These sectioned sample was then ground and polished for optical microscopic examination and nanoindentation studies. Figure 2b shows embedded intermetallics (indicated by the red dashed lines) in the alloy matrix.
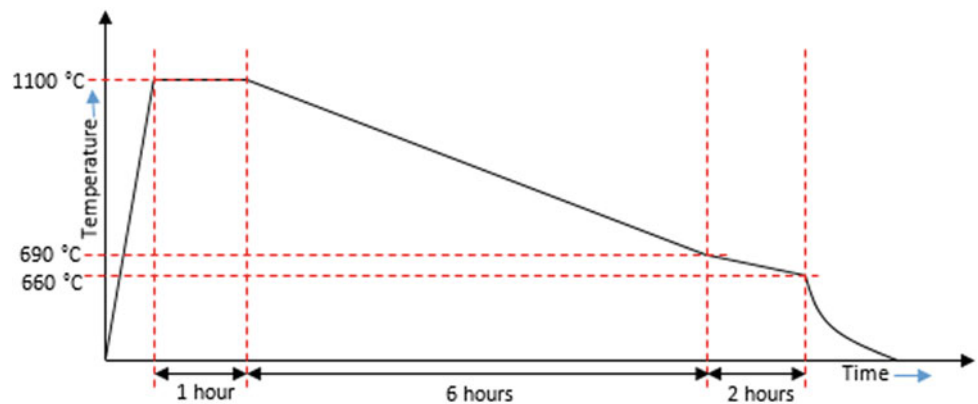
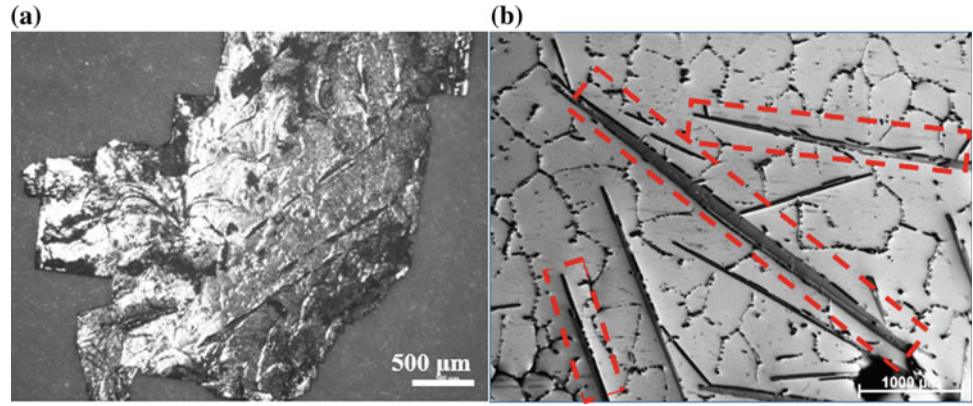Fig. 1 Thermal-cycle of an Al-3wt%Zr alloy formation

Fig. 2 Optical micrographs of Al$_3$Zr **a** extracted crystal, and **b** intermetallics embedded in Al matrix

Experimental Setup

Depth Sensing Indentation (DSI)

The embedded intermetallic specimen (Fig. 2b) was staged on a high temperature ultra nanoindentation system (UNHT HTV, Anton Paar, Switzerland) based on the principle of active surface referencing (note that we used only room-temperature measurements in this study). The detailed information related to the instrumentation is provided elsewhere [19]. A series of indents were employed onto the embedded intermetallics using a Berkovich diamond indenter at a constant loading and unloading rate of 20 mN/min with a dwell period of 5 s. The indentations were performed at room temperature conditions with data acquisition rate of 10 Hz. The load-displacement measurement of the Al$_3$Zr crystal was obtained for maximum load of 10 mN at room temperature. Other indentation types such as fracture mode were also performed over the specimen using a geometrically well-defined diamond cube corner indenter with a maximum load of 100 mN. Minimum 5 indents were performed for each measurement mode to provide statistically meaningful results.

Single Laser-Induced Bubble (LIB)

A single 10.5 ± 1 mJ (instrumental error), 6–8 ns high energy laser pulse using Nd:YAG laser system (Nano S 130-10, Litron Lasers, UK) was focused into deionised water, with enough energy to cause optical breakdown and subsequent generation of a laser bubble within a chamber of dimension 420 mm $\times$ 438 mm $\times$ 220 mm. Detailed information of the experimental setup can be found elsewhere [20]. The extracted intermetallic crystals were fixed on top of a steel base using a cyanoacrylate adhesive. The fixed crystals were then placed on a custom-built xyz manipulator and adjusted such that the laser bubble forms just beside the crystal. In situ recordings of the crystal-single bubble interaction were captured with high-speed shadowgraphic imaging with 500,000 frames per second using HPV X2 (Shimadzu, Japan) camera generating 256 frames per image sequence. The images shown in this paper have been confirmed after 5 repeated observations and are considered to be representative.

Results and Discussion

Depth Sensing Indentation of Primary Al$_3$Zr Crystal

Mechanical properties such as elastic modulus, hardness and fracture toughness of the Al$_3$Zr crystals were measured. The mechanical properties have been evaluated using the method introduced by Oliver and Pharr [21]. The maximum displacement of the indenter (h_{max}) was found to be around 237 nm upon loading and final depth after unloading the indenter was close to 181 nm. The contact stiffness during the unloading stage was 0.235 mN/nm.

The mechanical properties such as the hardness (H) and elastic modulus (E) were found to be in the range of 7.2–7.6 GPa and 194–206 GPa respectively. These values of H and E were found to be in good agreement with the existing data in the literature [20, 21]. Fracture toughness (K_c) of the crystal was found to be close to 1 MPa√m. Table 1 summarizes the material properties of Al$_3$Zr determined using the indentation measurements.

Table 1 Measured mechanical properties of Al$_3$Zr crystal using DSI technique

Mechanical properties	Measured value	Std. dev.
Hardness (GPa)	7.4	0.2
Elastic modulus (GPa)	200	5.8
Fracture toughness (MPa√m)	1.1	0.1

Fragmentation of Al₃Zr Crystal

Figure 3a-l shows the sequence of images captured during the fragmentation of a primary Al$_3$Zr crystal by a generated single LIB. Only selective images have been shown for the best representation of fragmentation mechanism. The first image at t = 0 μs shows the primary crystal of dimension approximately 5.7 mm × 4.7 mm × 0.1 mm with two pre-existing notches of length 0.4 mm and 0.35 mm (indicated with dashed arrows). At t = 2.5 μs, a laser bubble released a continuous band of shock waves that propagated through the liquid as shown in Fig. 3b, c and caused a crack of the length ≈ 0.4 mm to form at the encircled (yellow) position (at a distance of 4.8 mm from the emission centre). The laser bubble undergoes the expansion phase from t = 2.5 μs to t = 152.5 μs in reaction to energy disposition of the host medium and reached a maximum radius of 1.5 mm encircled in blue (Fig. 3d). After this, as the inertia of the bubble wall started to decelerate, the contraction phase of the laser bubble initiated, eventually causing the bubble to collapse at t = 332.5 μs thereby releasing another cycle of shock wave bands spreading over the liquid and ultimately attenuating over the distance from the emission centre. This is followed by multiple rebound oscillation and release of shock waves up to t = 617.5 μs until the bubble completely collapses.

It is interesting to note that after the release of the second cycle of shock wave bands upon the bubble collapse phase i.e. t = 335 μs (Fig. 3g) and subsequent growth of a rebound bubble i.e. t = 410 μs (Fig. 3h), a clear crack growth (encircled in red) can be seen. Crack initiated at one of the notches and propagated towards the other notch as shown in Fig. 3j causing complete fragmentation of the primary Al$_3$Zr crystal in Fig. 3l. Since there was no direct interaction of the laser bubble directly with the crystal, it seems that the whole fragmentation process was a result of generated and repeated shock waves emitted from the nucleation and collapse phase of the laser bubble.

Fracture Mechanism

It is important to quantify the fragmentation mechanism in order to have a better understanding of the observed phenomena discussed in section "Fragmentation of Al$_3$Zr Crystal". The fragmentation mechanics can be interpreted in terms of a critical stress required to completely fracture the crystal with a pre-existing crack/notch.

This section describes the typical Griffith crack growth analysis observed for the Al$_3$Zr crystal fragmented using the laser-induced bubble by the emitted shock waves. The basic mechanism underlined through the imaging observations points clearly towards the involvement of two-stage fracture that involves fatigue mechanism at the initial stages of crack growth until the crack size reaches its critical length followed by the brittle fracture mechanism in the final stages as has been also observed by Wang et al. [2]. Hence, it is of interest to understand the strength of shock wave in terms of associated pressure amplitude (P_r). The magnitude of the pressure amplitude variation over the distance from the
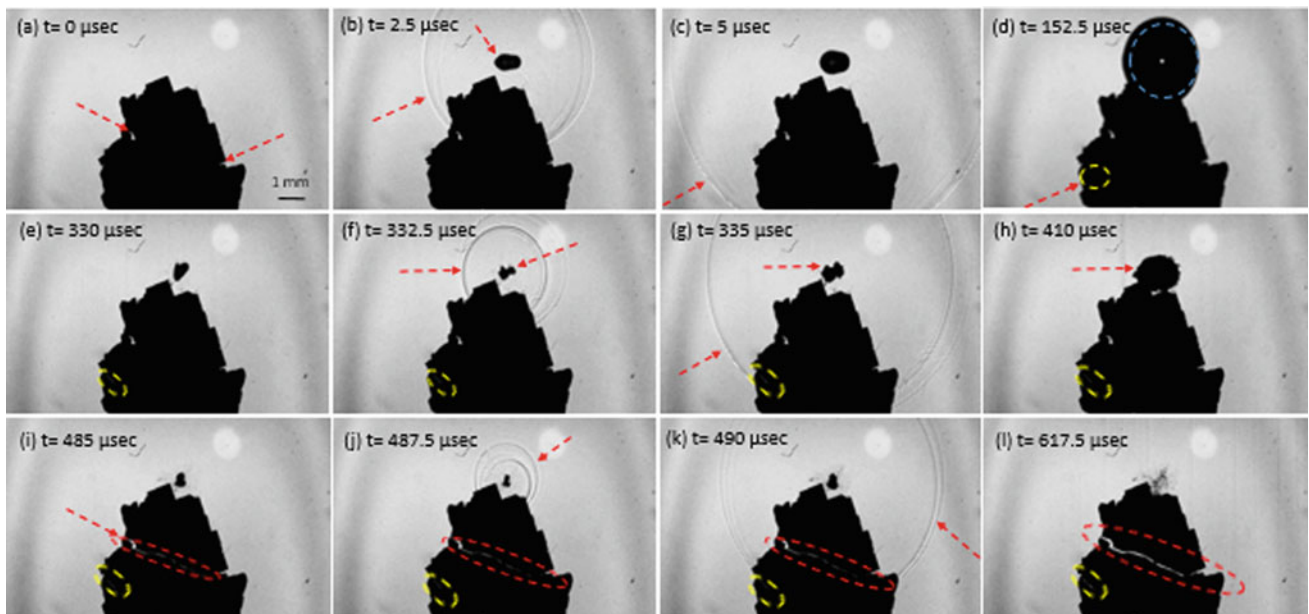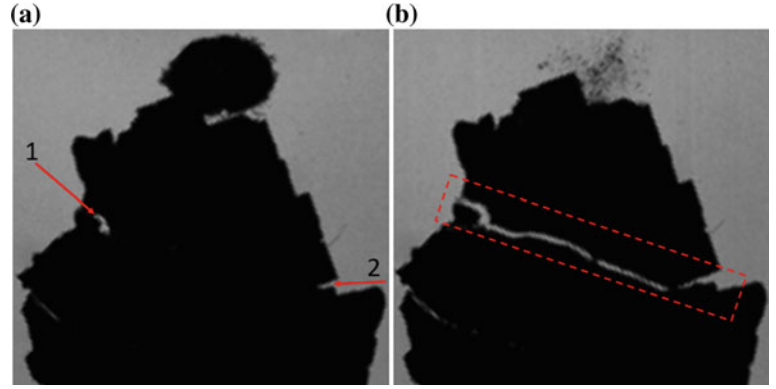

Fig. 3 Real time captured images of interaction of a laser nucleated single bubble inducing crack and subsequent fragmentation of primary Al$_3$Zr crystal recorded at 500,000 fps

Fig. 4 Images of Al$_3$Zr crystal just **a** before crack propagation and **b** after crack propagation caused by bubble collapse shock waves

shock wave emission centre has been considered to follow the relation suggested by Vogel et al. [22]. It has been observed that the shock pressure decays over distance, r following the relation:

$$P_r = c_1 \rho_o u_s \left(10^{(u_s - c_o)/c_2} - 1 \right) + P_\infty \qquad (1)$$

where ρ_o is the density of the medium (water) before shock wave emission, u_s is the shock wave velocity derived from the $r(t)$ curve, c_o is the speed of sound in water, c_1 is an empirical constant equal to 5190 m/s, $c_2 = 25306$ m/s and P_∞ denotes the hydrostatic pressure. It has been observed that the pressure amplitude close to 100 MPa is roughly proportional to r^{-1} near the shock front [23, 22].

Using the Griffith fracture criterion [24] for brittle materials, the applied stress needed for a given crack length of the notch was evaluated from the following expression:

$$K_c = C\sigma\sqrt{\pi a} \qquad (2)$$

where K_c is the fracture toughness of the material taken as 1.1 from the DSI measurements mentioned in section "Depth Sensing Indentation of Primary Al$_3$Zr Crystal", a is the notch length (0.4 mm), C is the constant depending on the crack length taken as 1.12 and σ is the stress required to cause complete fracture of material. For notch 1 formed during repeated expansion and collapse of a cavitation bubble (Fig. 4a), the stress needed to induce complete fracture was found to be 27 MPa as estimated by Eq. 2. Based on the distance of notch 1 from the bubble centre, pressure amplitude of the propagating shock front from a similarly collapsing bubble was determined to be 39 MPa considering that shock pressure decays as r^{-1} [22]. As a result, it can be confirmed that the shock wave emission from the expansion and collapse phase of a single bubble is adequate to cause brittle failure of a crystal in the vicinity.

Conclusions

Depth sensing indentation technique was used to evaluate the mechanical properties of the primary Al$_3$Zr crystals at room temperature. The hardness, elastic modulus and fracture toughness values indicated the extreme brittle nature of the intermetallic with values more or less consistent with data present in the literature. The primary Al$_3$Zr crystals were then extracted from a heavily etched Al-3wt% Zr alloy and in situ imaging of their fragmentation behaviour upon interaction with a laser induced singe bubble was conducted. Upon examining the in situ recorded high-speed images, the fragmentation mechanism of the crystal was explained both qualitatively and quantitatively using fracture mechanics. The fragmentation of the crystal occurs primarily by the emitted shock waves from the collapsing bubble. The fracture happens in two stages: (i) shock wave bands interact with the crystal present nearby periodically inducing a low cycle fatigue until a critical size crack is formed; (ii) the fracture happens shortly after, following a typical brittle failure mechanism. Pressure amplitudes in the range of 30–40 MPa were estimated to cause fragmentation of the studied crystals.

Future work includes the investigation of sonofragmentation and the associated mechanisms under ultrasonic excitation. Based on the current results we envisage that shock wave propagation should still be the dominant fracturing mechanism of intermetallics.

References

1. D. G. Eskin, I. Tzanakis, F. Wang, G. S. B. Lebon, T. Subroto, K. Pericleous, and J. Mi, "Fundamental studies of ultrasonic melt processing," *Ultrason. Sonochem.*, vol. 52, pp. 455–467, Apr. 2019.

2. F. Wang, I. Tzanakis, D. Eskin, J. Mi, and T. Connolley, "In situ observation of ultrasonic cavitation-induced fragmentation of the primary crystals formed in Al alloys," *Ultrason. Sonochem.*, vol. 39, no. March, pp. 66–76, 2017.

3. F. Wang, D. Eskin, T. Connolley, and J. Mi, "Effect of ultrasonic melt treatment on the refinement of primary Al3Ti intermetallic in an Al-0.4Ti alloy," *J. Cryst. Growth*, vol. 435, pp. 24–30, 2016.

4. G. I. Eskin and D. G. Eskin, "Production of natural and synthesized aluminum-based composite materials with the aid of ultrasonic (cavitation) treatment of the melt," *Ultrason. Sonochem.*, vol. 10, no. 4–5, pp. 297–301, Jul. 2003.

5. T. V. Atamanenko, D. G. Eskin, L. Zhang, and L. Katgerman, "Criteria of Grain Refinement Induced by Ultrasonic Melt Treatment of Aluminum Alloys Containing Zr and Ti," *Metall. Mater. Trans. A*, vol. 41, no. 8, pp. 2056–2066, Aug. 2010.

6. G. I. Eskin and D. G. Eskin, "Some control mechanisms of spatial solidification in light alloys," *Zeitschrift für Met.*, vol. 95, no. 8, pp. 682–690, Aug. 2004.

7. G. I. Eskin, "Broad prospects for commercial application of the ultrasonic (cavitation) melt treatment of light alloys," *Ultrason. Sonochem.*, vol. 8, no. 3, pp. 319–325, Jul. 2001.

8. G. M. Swallowe, J. E. Field, C. S. Rees, and A. Duckworth, "A photographic study of the effect of ultrasound on solidification," *Acta Metall.*, vol. 37, no. 3, pp. 961–967, Mar. 1989.

9. D. Shu, B. Sun, J. Mi, and P. S. Grant, "A High-Speed Imaging and Modeling Study of Dendrite Fragmentation Caused by Ultrasonic Cavitation," *Metall. Mater. Trans. A*, vol. 43, no. 10, pp. 3755–3766, Oct. 2012.

10. R. Chow, R. Blindt, A. Kamp, P. Grocutt, and R. Chivers, "The microscopic visualisation of the sonocrystallisation of ice using a novel ultrasonic cold stage," *Ultrason. Sonochem.*, vol. 11, no. 3–4, pp. 245–250, May 2004.

11. R. M. Wagterveld, L. Boels, M. J. Mayer, and G. J. Witkamp, "Visualization of acoustic cavitation effects on suspended calcite crystals," *Ultrason. Sonochem.*, vol. 18, no. 1, pp. 216–225, Jan. 2011.

12. B. Wang, D. Tan, T. L. Lee, J. C. Khong, F. Wang, D. Eskin, T. Connolley, K. Fezzaa, and J. Mi, "Ultrafast synchrotron X-ray imaging studies of microstructure fragmentation in solidification under ultrasound," *Acta Materialia*, vol. 144. pp. 505–515, 2018.

13. W. W. Xu, I. Tzanakis, P. Srirangam, S. Terzi, W. U. Mirihanage, D. G. Eskin, R. H. Mathiesen, A. P. Horsfield, and P. D. Lee, "In Situ Synchrotron Radiography of Ultrasound Cavitation in a Molten Al-10Cu Alloy," in *TMS 2015 144th Annual Meeting & Exhibition*, 2015, pp. 61–66.

14. F. Wang, D. Eskin, J. Mi, C. Wang, B. Koe, A. King, C. Reinhard, and T. Connolley, "A synchrotron X-radiography study of the fragmentation and refinement of primary intermetallic particles in an Al-35 Cu alloy induced by ultrasonic melt processing," *Acta Materialia*, vol. 141. pp. 142–153, 2017.

15. I. Tzanakis, W. W. Xu, G. S. B. Lebon, D. G. Eskin, K. Pericleous, and P. D. Lee, "In situ synchrotron radiography and spectrum analysis of transient cavitation bubbles in molten aluminium alloy," *Phys. Procedia*, vol. 70, no. 0, pp. 841–845, 2015.

16. W. W. Xu, I. Tzanakis, P. Srirangam, W. U. Mirihanage, D. G. Eskin, A. J. Bodey, and P. D. Lee, "Synchrotron quantification of ultrasound cavitation and bubble dynamics in Al-10Cu melts," *Ultrason. Sonochem.*, vol. 31, pp. 355–361, 2016.

17. I. Tzanakis, D. G. Eskin, A. Georgoulas, and D. K. Fytanidis, "Incubation pit analysis and calculation of the hydrodynamic impact pressure from the implosion of an acoustic cavitation bubble," *Ultrason. Sonochem.*, vol. 21, no. 2, pp. 866–878, 2014.

18. S. Zhen and G. J. Davies, "Observations of the growth morphology of the intermetallic compound Al3Zr," *J. Cryst. Growth*, vol. 64, no. 2, pp. 407–410, Nov. 1983.

19. M. Conte, G. Mohanty, J. J. Schwiedrzik, J. M. Wheeler, B. Bellaton, J. Michler, and N. X. Randall, "Novel high temperature vacuum nanoindentation system with active surface referencing and non-contact heating for measurements up to 800 °C," *Rev. Sci. Instrum.*, vol. 90, no. 4, p. 045105, Apr. 2019.

20. K. Johansen, J. H. Song, K. Johnston, and P. Prentice, "Deconvolution of acoustically detected bubble-collapse shock waves," *Ultrasonics*, vol. 73, pp. 144–153, 2017.

21. W. C. Oliver and G. M. Pharr, "An improved technique for determining hardness and elastic modulus using load and displacement sensing indentation experiments," *J. Mater. Res.*, vol. 7, no. 06, pp. 1564–1583, Jun. 1992.

22. A. Vogel, S. Busch, and U. Parlitz, "Shock wave emission and cavitation bubble generation by picosecond and nanosecond optical breakdown in water," *J. Acoust. Soc. Am.*, vol. 100, no. 1, pp. 148–165, Jul. 1996.

23. D. De Fontaine, "Cluster Approach to Order-Disorder Transformations in Alloys," *Solid State Phys.*, vol. 47, pp. 33–176, Jan. 1994.

24. M. Janssen, J. Zuidema, and R. Wanhill, *Fracture mechanics*. Spon Press, 2004.